

1 **Revision 2**

2 Regular article

3 **Lepageite, $\text{Mn}^{2+}_3(\text{Fe}^{3+}_7\text{Fe}^{2+}_4)\text{O}_3[\text{Sb}^{3+}_5\text{As}^{3+}_8\text{O}_{34}]$, a new arsenite-antimonite mineral from the**
4 **Szklary pegmatite, Lower Silesia, Poland**

5
6 **Lepageite, a new arsenite–antimonite mineral from the Szklary pegmatite, Lower Silesia,**
7 **Poland**

8
9 **ADAM PIECZKA^{1*}, MARK A. COOPER² AND FRANK C. HAWTHORNE²**

10
11 ¹AGH University of Science and Technology, Department of Mineralogy, Petrography
12 and Geochemistry, 30-059 Kraków, Mickiewicza 30, Poland

13 ²Department of Geological Sciences, University of Manitoba, Winnipeg, Manitoba R3T 2N2,
14 Canada; mark_cooper@umanitoba.ca, frank_hawthorne@umanitoba.ca

15
16 * *Corresponding author:* pieczka@agh.edu.pl

17
18 **Abstract**

19 Lepageite, a new arsenite-antimonite mineral, was discovered in a granitic pegmatite hosted by
20 serpentinites of the Szklary massif, Lower Silesia, SW Poland. The mineral occurs as euhedral to
21 subhedral, brownish-black, opaque, sometimes twinned crystals up to 20–30 μm in size
22 (commonly only $\sim 5 \mu\text{m}$), with metallic luster. Average microprobe analysis (in wt%): As_2O_3
23 31.61, Sb_2O_3 26.23, $\text{Fe}_{\text{total}}\text{O}$ 29.79 (Fe_2O_3 21.51 + FeO 10.74 from stoichiometry), MnO 8.44,

24 MgO 0.26, sum 98.49, based on 37 O and 13 As + Sb *apfu* gives the empirical formula
25 $(\text{Fe}^{3+}_{6.90}\text{Fe}^{2+}_{3.89}\text{Mn}^{2+}_{3.10}\text{Mg}_{0.16})_{\Sigma 14.05}(\text{As}^{3+}_{8.32}\text{Sb}^{3+}_{4.68})_{\Sigma 13.00}\text{O}_{37}$, corresponding to the end-member
26 lepageite formula $\text{Mn}^{2+}_3(\text{Fe}^{3+}_7\text{Fe}^{2+}_4)\text{O}_3[\text{Sb}^{3+}_5\text{As}^{3+}_8\text{O}_{34}]$. Streak, hardness, tenacity, optical
27 properties and density were not determined due to the tiny grain size and very small amount of
28 available material. The mineral does not show fluorescence, and no cleavage, fracture or parting
29 were observed. Lepageite is triclinic, space group *P*-1, and has unit-cell parameters $a =$
30 $10.607(3)$, $b = 10.442(3)$, $c = 15.260(5)$ Å, $\alpha = 89.579(12)$, $\beta = 104.479(8)$, $\gamma = 89.706(9)^\circ$, $V =$
31 $1636.4(9)$ Å³, $Z = 2$. The density calculated on the basis of the empirical lepageite composition
32 and its unit-cell volume is 5.192 g/cm³. The crystal structure was refined to an R_1 index of 3.6%.
33 Four Sb^{3+}O_4 groups link to four As^{3+}O_3 groups to form a cluster of composition
34 $[\text{Sb}_4\text{As}_4\text{O}_{19}][\text{AsO}_3]_5$ that consists of a six-membered ring of alternating Sb^{3+}O_4 and As^{3+}O_3
35 polyhedra linked to a three-membered ring of two Sb^{3+}O_4 and one As^{3+}O_3 polyhedra that is
36 decorated by another As^{3+}O_3 polyhedron. There are also five distinct isolated As^{3+}O_3 groups.
37 These units link to densely packed arrangements of FeO_6 octahedra, MnO_7 and MnO_8 polyhedra
38 to form a strongly bonded framework. The strongest lines in the X-ray powder diffraction pattern
39 of lepageite, calculated on the basis of the proposed structure model, are, respectively [d in Å, I ,
40 (hkl)]: 2.831, 100, (0 -3 3); 2.854, 92, (0 3 3); 2.846, 88, (3 0 2); 2.898, 85, (-3 0 4); 2.487, 34, (-3
41 -3 1); 2.474, 34, (-3 3 1) and 2.463, 34, (0 0 6). Lepageite is a primary mineral formed during
42 injection of an evolved LCT-type melt related to anatectic processes within the metasedimentary-
43 metavolcanic complex of the nearby Góry Sowie Block, ~380 Ma, into serpentinite of the
44 Szklary massif and its contamination by fluid-mobile serpentinite-hosted elements, among others
45 As and Sb, transported in the form of H_2AsO_3^- and HSbO_2 species at $\text{pH} \approx 9-11$ and a low redox
46 potential of -0.7 to -0.3 V.

47

48 **Keywords:** lepageite, new mineral, arsenite, antimonite, chemical composition, crystal structure,
49 crystallization conditions, Szklary, Poland.

50

51

Introduction

52 The Szklary pegmatite is a small body of granitic LCT (Li–Cs–Ta) pegmatite hosted by
53 serpentinites of the Szklary massif, Lower Silesia, Poland. It is considered to be part of the
54 tectonically fragmented Sudetic ophiolite (Majerowicz and Pin 1986) and is about 420 Ma old
55 (Oliver et al. 1993). In spite of its small dimensions, the pegmatite is notable due to (i) the
56 presence of many rare and unknown minerals of various mineral groups, e.g., native metals and
57 metalloids, Nb-Ta and Mn oxides, Mn phosphates with the apatite-group and graffonite-group
58 minerals richest in Mn worldwide, numerous As-Sb accessory phases in the absence of typical
59 löllingite and arsenopyrite; (ii) very high degrees of Mn-Fe fractionation; and (iii) the absence of
60 sulfides and the occasional presence of baryte as the only phase containing sulfur (Pieczka 2010;
61 Pieczka et al. 2011, 2013, 2015, 2018; Szuszkiewicz et al. 2018).

62 The assemblage of As-Sb minerals in the pegmatite (Table 1) evolves from zero-valent native
63 As and Sb and their melts, through various As^{3+} and Sb^{3+} phases to pyrochlore-supergroup
64 minerals in which As and Sb may occur also as pentavalent cations, and finally to As^{5+}
65 substituting for P^{5+} in some phosphates. Such a sequence indicates the crystallization of the
66 assemblage at varying Eh-pH conditions. Thus, considering valence states of As and Sb and other
67 coexisting cations, the assemblage provides an opportunity to evaluate its formation conditions.
68 In the paper, we discuss these conditions based on the composition of a newly discovered
69 arsenite-antimonite mineral lepageite, ideally $\text{Mn}^{2+}_3(\text{Fe}^{3+}_7\text{Fe}^{2+}_4)\text{O}_3[\text{Sb}^{3+}_5\text{As}^{3+}_8\text{O}_{34}]$. Lepageite has
70 been approved by the Commission on New Minerals, Nomenclature and Classification
71 (CNMNC) of the International Mineralogical Association (IMA 2018–028). The name of the

72 mineral is for Yvon Le Page (born October 7, 1943), a crystallographer who (1) developed the
73 program MISSYM that has played a major role in the correct solution of complex mineral
74 structures (including lepageite itself), and (2) solved the structures of many minerals and was
75 involved in the description of several new minerals. The lepageite holotype (specimen Sz 96) is
76 deposited in the collection of the Mineralogical Museum of University of Wrocław, catalogue
77 number MMWr IV7926. The postal address of the museum is as follows: University of Wrocław,
78 Faculty of Earth Science and Environmental Management, Institute of Geological Sciences,
79 Mineralogical Museum, 50-205 Wrocław, Cybulskiego 30, Poland.

80

81

Occurrence

82 Lepageite was discovered in the Szklary LCT pegmatite (50°39.068'N, 16°49.932'E), ~ 6 km N
83 of the Ząbkowice Śląskie town, ~60 km south of Wrocław, Lower Silesia, SW Poland. The
84 massif is part of the Central-Sudetic ophiolite that adjoins the Góry Sowie Block (GSB) on the
85 east. It is enclosed as a mega-boudin in the mylonitized GSB gneisses of the Early Carboniferous
86 Niemcza Shear Zone. The pegmatite, completely excavated by mineral collectors in 2002, formed
87 a NNE-SSW elongated lens or a boudin ~4×1 m in planar section, outcropped in the northern part
88 of the massif. To the southwest, it has a primary intrusive contact with an altered aplitic gneiss up
89 to 2 m thick, and both rocks are surrounded by tectonized serpentinite (Szuskiewicz et al. 2018).
90 A vermiculite-chlorite-talc zone is locally present along the contact with serpentinite. The
91 pegmatite corresponds to the beryl–columbite–phosphate subtype of the *REL*-Li pegmatite class
92 in the classification of Černý and Ercit (2005). The pegmatite [383±2 Ma; CHIME dating on
93 monazite-(Ce), Pieczka et al. 2015] is significantly older than the neighboring small late-
94 syntectonic dioritic, syenitic and granodioritic intrusions (~335–340 Ma) occurring in the

95 Niemcza Shear Zone (Oliver et al. 1993), and corresponds to the anatectic event in the adjacent
96 GSB of 380–374 Ma (van Breemen et al. 1988; Timmermann et al. 2000; Turniak et al. 2015).

97 The pegmatite consists mainly of plagioclase ($Ab_{99-82}An_{1-18}$), microcline perthite, quartz and
98 biotite, with minor Fe^{3+} -bearing schorl-dravite, spessartine and muscovite. It is relatively poorly
99 zoned with (1) a marginal graphic zone composed of albite + quartz \pm minor-to-accessory biotite
100 commonly altered to clinocllore + black tourmaline; (2) a coarser-grained intermediate graphic
101 zone of microcline perthite + quartz + small quartz-tourmaline nests, with smaller amounts of
102 albite and biotite, increased abundance of muscovite and spessartine, and accessory chrysoberyl
103 present locally in muscovite aggregates; (3) a central zone of graphic microcline + quartz, in
104 places developed as blocky feldspar with interstitial albite, rare muscovite, and no black
105 tourmaline or biotite (Pieczka 2000; Pieczka et al. 2015). The aforementioned accessory minerals
106 are present in zones (2) and (3). Most of them form crystals usually less than 1 mm in size,
107 disseminated in quartz, microcline, albite and muscovite.

108 Lepageite is an accessory mineral, occurring only as minute inclusions, reaching 30 μm in
109 diameter (commonly $\sim 5 \mu m$), in (Mn,Be,Na,Cs)-bearing cordierite or close to it (Fig. 1). It is
110 associated with other Fe-Mn-As-Sb oxides: schafarzikite and three or four unrecognized arsenite-
111 antimonite phases of different (Fe+Mn)/(As+Sb) ratio, but rarer and even smaller than lepageite,
112 harmotome, Ba-bearing microcline, baryte and hematite. The (Cs,Mg)-bearing beryl, (Cs,Mg)-
113 bearing muscovite, Cs-bearing phlogophite and annite, paragonite, clinocllore, chamosite,
114 vermiculite and smectites are found as the replacement and breakdown products after cordierite.

115

116 **Physical properties**

117 Lepageite forms small euhedral to subhedral, brownish-black, opaque crystals up to 20–30 μm in
118 size, with metallic luster (Fig. 1). Due to the tiny grain sizes and very small amount of available

119 material, streak, hardness, tenacity and optical properties were not determined. The mineral does
120 not show fluorescence, and no cleavage, fracture or parting were observed. Density was not
121 measured for the same reasons; the density calculated on the basis of the empirical composition
122 of the type lepageite and its unit-cell volume is 5.192 g/cm³. Using the empirical formula and
123 calculated density, the mean refractive index obtained from Gladstone-Dale relation (Mandarino
124 1979, 1981) is 2.21.

125

126 **Chemical composition**

127 Quantitative chemical analyses of lepageite were done at the Inter-Institute Analytical Complex
128 for Minerals and Synthetic Substances at the University of Warsaw, Poland, using a Cameca SX
129 100 electron microprobe operating in wavelength-dispersive (WDS) mode with an accelerating
130 voltage of 15 kV, a beam current of 10 nA, peak count-time of 20 s, background time of 10 s, and
131 a beam diameter of 1-2 μm. Standards, analytical lines, diffracting crystals and mean detection
132 limits (wt%) were as follows: diopside (Mg Kα, TAP, 0.03), rhodonite (Mn Kα, LIF, 0.10),
133 hematite (Fe Kα, LIF, 0.10), GaAs (As Lα, TAP, 0.06) and InSb (Sb Lα, PET, 0.08). Aluminum,
134 Si, P, Ti, Nb and Ta were sought but were below the detection limits. The raw data were reduced
135 with the PAP routine of Pouchou and Pichoir (1985). Analytical data on holotype material are
136 given in Table 2. The empirical formula of lepageite,

137 $(\text{Fe}^{3+}_{6.90}\text{Fe}^{2+}_{3.89}\text{Mn}^{2+}_{3.10}\text{Mg}_{0.16})_{\Sigma 14.05}(\text{As}^{3+}_{8.32}\text{Sb}^{3+}_{4.68})_{\Sigma 13.00}\text{O}_{37}$, was calculated on the basis of 37 O
138 atoms per formula unit (*apfu*) and 13 As³⁺ + Sb³⁺ cations as indicated by the crystal structure of
139 the mineral. Taking into account the results of the crystal-structure investigation (see below), the
140 end-member formula of lepageite is $\text{Mn}^{2+}_3(\text{Fe}^{3+}_7\text{Fe}^{2+}_4)\text{O}_3[\text{Sb}^{3+}_5\text{As}^{3+}_8\text{O}_{34}]$, corresponding to (in
141 wt%): As₂O₃ 30.68, Sb₂O₃ 28.26, Fe₂O₃ 21.67, FeO 11.14, and MnO 8.25.

142

143
144
145
146
147
148
149
150
151
152
153
154
155
156
157
158
159
160
161
162
163
164
165
166

Powder diffraction data

Powder diffraction data could not be collected due to scarcity of material. The X-ray powder diffraction pattern calculated from the refined crystal-structure is reported in Table 3.

Crystal structure

A single grain, $7 \times 20 \times 30 \mu\text{m}$ and composed of two twinned crystals, was extracted; all other grains were < 5 microns. The grain was an entirely entombed inclusion that needed to be physically broken out. Therefore, we coated the section with grease to avoid loss of the crystal during this process.

Data collection and refinement

The extracted grain was attached to a MiTeGen polymer loop and mounted on a Bruker D8 three-circle diffractometer equipped with a rotating-anode generator ($\text{MoK}\alpha$ X-radiation), multilayer optics and an APEX-II detector. A Ewald sphere of data was collected to $62^\circ 2\theta$ using 20 s per 0.2° frame with a crystal-detector distance of 5 cm. Evaluation of the diffraction pattern revealed that the crystal contained a significant non-merohedral twin-component (180° rotation about c^*), and the intensity data were processed as an overlapping twin. Twin integration gave 94434 total reflections, with 32990 [component 1], 32911 [component 2] and 28533 [both components] (*Deposit Material*). The reflections were averaged and merged [$R_{\text{int}} = 5.0\%$] to give 10478 reflections (single reflections from the primary domain, plus composites involving both domains) for structure (twin) refinement. The unit-cell dimensions were obtained by least-squares refinement of 4073 reflections with $I > 10\sigma I$. All diffraction maxima from the X-ray crystal can be indexed on the triclinic cell with the inclusion of the twin law $[-0.998 -0.001 0.005 / 0.000 - 1.000 -0.002 / 0.729 -0.025 0.998]$. The E statistics are consistent with a centre of symmetry, but attempts to solve the structure in the space group $P-1$ were unsuccessful. The atomic arrangement

167 was solved in $P1$, and a center of symmetry was subsequently identified using the MISSYM
168 program (Le Page 1987, 1988). An origin shift was applied and equivalent sites for the $P1$ model
169 were combined to produce the $P-1$ structure model. Structure (twin) refinement from 10478
170 reflections (including 6350 composites) gave a final R_1 value of 3.6% (for 9912 observed
171 reflections, $F_o > 4\sigma F$). The twin-volume fraction (i.e., twin contribution to composites) refined to
172 0.4756(7). Atom positions, equivalent isotropic-displacement parameters and selected interatomic
173 distances there are in the attached CIF file. Bond valences are given in Table 4.

174 **Site assignment**

175 The crystal structure of lepageite contains 28 cation sites and 37 anion sites. Lepageite is a simple
176 oxide, in that the bond-valence sums at all O sites are in the range 1.85–2.14 vu (valence unit)
177 (Table 4) and the O sites are occupied by simple O^{2-} ions. The cation sites can be subdivided into
178 two groups: (1) those with a heavier scattering species, i.e., $\geq 33 e$, with the cation displaced to
179 one side of three or four O-sites; and (2) those possessing a lighter scattering species, i.e., $\leq 26 e$
180 that is centrally located with a [6]- to [8]-coordination. In the first group, the sites are occupied by
181 As^{3+} and Sb^{3+} that show lone-pair-stereoactive behavior; in the second group, the sites are
182 occupied by Fe^{3+} , Fe^{2+} and Mn^{2+} .

183 The Sb(1)–Sb(4) sites are occupied by Sb^{3+} with two short equatorial bonds to O_{eq} (i.e., 1.93–
184 2.03 Å) and two slightly longer axial bonds to O_{ax} (i.e., 2.12–2.35 Å), all lying to one side of the
185 Sb^{3+} cation. The O_{ax} –Sb– O_{ax} angles vary from 141.9–145.4°, and the O_{eq} –Sb– O_{eq} angles vary
186 from 95.3–105.7°. A similar coordination for Sb^{3+} occurs in stenhuggarite (Coda et al. 1977).

187 Both the refined scattering and observed $\langle^{[4]}Sb-O\rangle$ distances (i.e., 2.120–2.129 Å) are consistent
188 with full occupancy of these sites by Sb^{3+} . There are longer Sb-O distances in each coordination
189 polyhedron, resulting in the coordination numbers [6] and [7] $\times 3$, respectively. These longer
190 bonds contribute significantly to the sum of the incident bond-valences about the central cations,

191 bringing the sums into accord with the valence-sum rule. The observed $\langle^{[6]}\text{Sb}^{3+}-\text{O}^{2-}\rangle$ and
192 $\langle^{[7]}\text{Sb}^{3+}-\text{O}^{2-}\rangle$ distances are in accord with the mean distances observed in all inorganic oxide-
193 oxysalt Sb^{3+} structures (Gagné and Hawthorne 2018): grand $\langle^{[6]}\text{Sb}^{3+}-\text{O}^{2-}\rangle = 2.443 \text{ \AA}$, range:
194 $2.349\text{--}2.623 \text{ \AA}$; $\langle^{[7]}\text{Sb}^{3+}-\text{O}^{2-}\rangle = 2.486 \text{ \AA}$, range: $2.445\text{--}2.517 \text{ \AA}$.

195 The As(1)–As(9) sites are occupied dominantly by As^{3+} [with minor Sb^{3+} at As(8) and As(9)],
196 with three short As-O bonds (i.e., $1.709\text{--}1.888 \text{ \AA}$) to one side of the As^{3+} ion. This is a typical
197 coordination for As^{3+} showing lone-pair-stereoactive behavior (e.g., Cooper and Hawthorne
198 1996, 2016). The refined scattering and $\langle^{[31]}\text{As}-\text{O}\rangle$ distances (i.e., $1.783\text{--}1.806 \text{ \AA}$) for the As(1)–
199 As(7) sites are consistent with full occupancy by As^{3+} . Scattering in excess of 33 electrons was
200 observed at the As(8) site, along with elongated As(8)-O bonds (i.e., $\langle^{[31]}\text{As}(8)-\text{O}\rangle = 1.878 \text{ \AA}$).
201 Site-occupancy refinement with coupled As and Sb scattering factors gave $\text{As}_{0.637}\text{Sb}_{0.363}$ for the
202 As(8) site. The excess scattering and longer bond-lengths are in accord with the refined Sb
203 content at As(8). The electron scattering around the As(9) site was modeled as two distinct sites
204 [As(9a) and As(9b)] with a refined As(9a)–As(9b) distance of $0.640(19) \text{ \AA}$. The refined site-
205 occupancies for the As(9a) and As(9b) sites are $1.034(7)$ and $0.071(7)$, respectively; as the sum
206 exceeds unity, the minor presence of an additional heavier scattering-species is indicated (i.e.,
207 Sb). The combined site-scattering of $36.5 e$ is consistent with an occupancy of $\text{As}_{0.81}$ and $\text{Sb}_{0.19}$
208 over the combined As(9a)/As(9b) sites. The As(9a) site has three short bonds to O ($\langle\text{As}(9a)-\text{O}\rangle =$
209 1.837 \AA) and the As(9b) site has two shorter and two intermediate bonds to O (similar to the Sb
210 sites). If the partitioning of As and Sb onto As(9a) and As(9b) is done with respect to ideal bond-
211 valence constraint (i.e., 3 vu) at both sites, then the inferred occupancies of $^{\text{As}(9a)}(\text{As}_{0.80}\text{Sb}_{0.17})_{\Sigma 0.97}$
212 and $^{\text{As}(9b)}(\text{As}_{0.01}\text{Sb}_{0.02})_{\Sigma 0.03}$ result. The As and Sb contents from the chemical analysis is
213 $(\text{As}_{8.32}\text{Sb}_{4.68})_{\Sigma=13}$ and from the site-occupancy refinement is $(\text{As}_{8.45}\text{Sb}_{4.55})_{\Sigma=13}$. For the sites
214 occupied solely by As^{3+} [As(1)–As(7)], the mean bond-lengths for a coordination of [3] are very

215 close and the incident bond-valence sums are close to 3 *vu*. Gagné and Hawthorne (2018) list the
216 grand $\langle [^{31}\text{As}^{3+}\text{-O}^{2-}] \rangle$ distance as 1.789 Å with a range of 1.758 to 1.794 Å, and the values found
217 here (1.759–1.789 Å) fall within this range. There are longer $\text{As}^{3+}\text{-O}^{2-}$ distances with suitable
218 geometry that could correspond to weakly bonded ligands but they do not contribute significantly
219 to the incident bond-valence sums.

220 There are three Mn sites occupied by Mn^{2+} . The Mn(1) and Mn(3) sites are coordinated by
221 eight O^{2-} ions with $\langle \text{Mn-O} \rangle$ distances of 2.472 and 2.436 Å, respectively. These two Mn
222 coordinations show significant overall bond-length dispersion, with individual Mn-O distances
223 spanning 2.09–3.10 Å. The Mn(2) site is coordinated by seven O atoms with a $\langle \text{Mn(2)-O} \rangle$
224 distance of 2.300 Å. The refined site-occupancy at Mn(2) [1.065(7)] indicates that a minor
225 amount of a heavier scattering species may be present (presumably Fe^{2+}). There are eleven Fe
226 sites octahedrally coordinated by O atoms with $\langle \text{Fe-O} \rangle$ distances in the range 2.023–2.153 Å.
227 The refined site-occupancies and mean bond-lengths are consistent with occupancy by a
228 combination of Fe^{3+} and Fe^{2+} . The Fe(1)–Fe(6) sites have $\langle \text{Fe-O} \rangle$ distances from 2.023–2.052 Å
229 and bond-valence sums (using the $\text{Fe}^{3+}\text{-O}$ equation) from 2.84–2.99 *vu* (Table 4), indicating that
230 these six Fe sites are predominantly occupied by Fe^{3+} . The Fe(9)–Fe(11) sites have $\langle \text{Fe-O} \rangle$
231 distances from 2.139–2.153 Å and bond-valence sums (using the $\text{Fe}^{2+}\text{-O}$ bond-valence
232 parameters) from 2.04–2.08 *vu* (Table 4), indicating that these three Fe sites are predominantly
233 occupied by Fe^{2+} . The Fe(7) and Fe(8) sites have intermediate $\langle \text{Fe-O} \rangle$ distances of 2.106 and
234 2.124 Å and bond-valence sums (using the $\text{Fe}^{3+}\text{-O}$ bond-valence parameters) of 2.53 and 2.33 *vu*,
235 respectively (Table 4), indicating that these two Fe sites are occupied by both Fe^{2+} and Fe^{3+} . All
236 As and Sb in the structure occur in coordinations characteristic of the 3+ oxidation state. The
237 three larger coordination polyhedra contain Mn that must be in the 2+ oxidation state as indicated
238 by the $\langle \text{Mn-O} \rangle$ distances that are characteristic of Mn^{2+} and are in accord with both the

239 electroneutrality of the structure and crystallization at low Eh conditions (see Genetic
240 Implications).

241 **Bond topology**

242 The various cation polyhedra are named using the central site. Sb(1), Sb(2), Sb(3), Sb(4) and
243 As(1), As(2), As(4), As(7) form a finite cluster of SbO₄ and AsO₃ groups (Fig. 2). Sb(2)O₄,
244 As(4)O₃, Sb(3)O₄, As(2)O₃, Sb(4)O₄ and As(1)O₃ form a six-membered ring by sharing
245 polyhedron corners with each other. The polyhedra are oriented with respect to the ring such that
246 the stereoactive lone-pairs of electrons belonging to the Sb³⁺ ions are oriented inward toward the
247 centre of the ring whereas the stereoactive lone-pairs of electrons belonging to the As³⁺ ions
248 are oriented outward away from the centre of the ring (Fig. 2). An Sb(1)O₄ group shares anions
249 with an Sb(3)O₄ group and an As(2)O₃ group to form a three-membered ring that shares an edge
250 with the six-membered ring, and the Sb(1)O₄ group links to a (terminal) As(7)O₃ group. All
251 AsO₃ groups in this cluster link only to SbO₄ groups whereas Sb(1)O₄ links directly to Sb(3)O₄ in
252 the three-membered ring (Fig. 2). All short As-O distances of the polyhedra in the cluster are
253 close to their mean value of 0.98 *vu*. However, the short Sb-O distances fall into two groups, with
254 pairs of bonds in each cluster close to their mean values of 0.88 and 0.48 *vu*, respectively. It is the
255 longer Sb-O bonds (*vu* ~ 0.48 *vu*) that link to the adjoining AsO₃ groups, allowing the bridging
256 anions also to link to the Fe and Mn octahedra. The remaining AsO₃ groups involve As(3),
257 As(5), As(6), As(8) and As(9), and are all isolated groups in that they do not link to each other or
258 to the polyhedra of the cluster. Thus, there is no direct linkage of AsO₃ polyhedra in the structure
259 of lepageite, and we may write the (Sb,As) component of the structure as [Sb₄As₄O₁₉][AsO₃]₅.

260 In the structure, Mn²⁺ is both [7]- and [8]-coordinated (Fig. 3a). The polyhedra share edges to
261 form a cluster of six polyhedra that are centered at the origin of the structure. Three Fe²⁺
262 octahedra, Fe(5), Fe(8) and Fe(9), share edges to form a staggered trimer (Fig. 3b). The

263 remaining Fe octahedra form an extended group of staggered chains of edge-sharing and corner-
264 sharing octahedra linked together by sharing corners with single octahedra (Fig. 4a,b). These
265 three elements form a densely packed framework with the Sb^{3+} and As^{3+} polyhedra (Fig. 5).

266 **Chemical formula**

267 The O(1)–O(27) anions are the twenty-seven O atoms involved in the nine AsO_3 groups. The
268 anions O(30), O(31), O(33) and O(34) form short bonds with Sb^{3+} at Sb(2) and Sb(4), and
269 collectively can be represented as two SbO_2 groups. The anions O(28), O(29) and O(32) form
270 short bonds with Sb(1) and Sb(3) where O(29) is a bridging O atom, thus forming a Sb_2O_3 group.
271 The remaining anions O(35), O(36) and O(37) form stronger bonds to the Mn and Fe sites. The
272 Mn^{2+} is highly ordered at the three Mn sites, whereas there is some disorder in the Fe^{2+} - Fe^{3+}
273 distribution. The divalent cations from the chemical analysis involve 3 elements (Fe^{2+} , Mn^{2+} ,
274 Mg^{2+}), and the overall 2+ and Fe^{3+} content is fixed by stoichiometry in relation to the constituent
275 37 O *apfu*. Thus, for $(\text{As}^{3+}, \text{Sb}^{3+})_{13}(\text{Fe}^{3+}, \text{Fe}^{2+}, \text{Mn}^{2+}, \text{Mg})_{14}\text{O}_{37}$, the Fe^{3+} content must be 7 *apfu*, and
276 the chemical data were so normalized. The formula $\text{Mn}^{2+}_3(\text{Fe}^{3+}_7\text{Fe}^{2+}_4)\text{O}_3[\text{Sb}^{3+}_4\text{As}^{3+}_9\text{O}_{34}]$ conveys
277 these attributes. Lepageite is in class 04.JA. Arsenites, antimonites, bismuthites; without
278 additional anions, without H_2O in the classification of Strunz (Strunz and Nickel 2001), and in
279 the classification of Dana (Gaines et al. 1997), it belongs to class 45. Acid and normal
280 antimonites and arsenites.

281

282 **Genetic implications**

283 Arsenites and antimonites are rare in Nature (< 50 mineral species) and are generally related to
284 base-metal and polymetallic ore deposits, usually as accessory phases associated with more
285 common As and Sb minerals such as arsenopyrite, löllingite, tetrahedrite, *etc.*. Of the ~20 arsenite
286 ± antimonite minerals of Fe ± Mn, only karibibite and schneiderhöhnite have been discovered in

287 pegmatites: karibibite, $\text{Fe}^{3+}_3(\text{As}^{3+}\text{O}_2)_4(\text{As}^{3+}_2\text{O}_5)(\text{OH})$, firstly at Tuften, Norway (Larsen 2013),
288 and karibibite + schneiderhöhnite, $\text{Fe}^{2+}\text{Fe}^{3+}_3\text{As}^{3+}_5\text{O}_{13}$, in pegmatites of the Kalba Range,
289 Kazakhstan (Voloshin et al. 1989). The arsenites were also found in the Urucum and Almerindo
290 pegmatite mines and the Boca Rica claim, Minas Gerais, Brazil (Cassedanne 1986; mindat.org),
291 and in the White Elephant Mine, South Dakota, USA (Smith and Fritzsich 2000). In almost all
292 occurrences, they are associated with löllingite \pm arsenopyrite \pm tennantite. Lepageite and
293 schafarzikite, from the Szklary pegmatite in Poland, are the third and fourth Fe-Mn arsenite-
294 antimonite species known from a pegmatitic environment. Moreover, in the Szklary pegmatite,
295 they coexist with three or four other Mn-Fe arsenite-antimonite species of different
296 $(\text{Mn}+\text{Fe})/(\text{As}+\text{Sb})$ ratio, still as yet undescribed due to their extremely small grain size. In this
297 locality, lepageite and the other arsenite-antimonite phases crystallized from a geochemically
298 evolved LCT-type melt related to anatectic melting in the nearby metasedimentary-metavolcanic
299 GSB complex, emplaced into serpentinites of the Szklary massif as an adjacent part of the
300 Sudetic ophiolite (Pieczka et al. 2015). The melt was strongly contaminated with Mg and
301 enriched in fluid-mobile elements, particularly As and Sb, by interaction with the host
302 serpentinite (see discussion on mobile elements in Deschamps et al. 2013; p.118). All these As
303 and Sb minerals formed prior to the crystallization of beryl and cordierite-group minerals, and
304 metasomatic alteration of the latter into an assemblage of (Mg,Cs)-enriched secondary beryl,
305 mica-, chlorite- and smectite-vermiculite-group minerals.

306 Characterization of the crystallization conditions for the arsenite-antimonite assemblage is an
307 interesting problem as the Szklary pegmatite is unique with regard to the relatively numerous As
308 \pm Sb phases present. As arsenite-antimonite minerals are extremely rare in pegmatites, their
309 appearance should be controlled by the As and Sb concentrations in pegmatite-forming melts,
310 along with the coexisting S and accompanying redox conditions. Typical pegmatite-forming

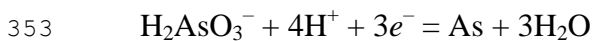
311 melts are usually poor in As and Sb, and these elements are generally completely incorporated by
312 löllingite and arsenopyrite that form at high temperature early in the crystallization of a
313 pegmatite. Geochemical fractionation can increase the concentrations of As and Sb to such a
314 degree that, in the final stages of pegmatite formation at relatively high oxygen fugacity, they
315 form Sb(As)-Nb-Ta oxides such as stibiocolumbite and stibiotantalite, or primary Sb-bearing
316 pyrochlore-supergroup minerals, e.g., oxystibiomicrolite or members of the roméite group. The
317 latter minerals involve partly or completely oxidized As and Sb. A good example of such
318 behaviour are the well-known pegmatites at Varuträsk (Sweden) with löllingite, arsenopyrite,
319 stibnite, native Sb, stibarsen, senarmontite, stibiotantalite and oxystibiomicrolite (Černý et al.
320 2004; Sandström 2008), at Viitaniemi (Finland) with löllingite, arsenopyrite, stibnite, tetrahedrite,
321 native Sb, senarmontite, valentinite and oxyplumboroméite (Sandström and Lahti 2009), at
322 Urucum (Brazil), where karibibite and schneiderhöhnite are associated with löllingite, tennantite
323 and stibiotantalite (Cassedanne 1986), and at the White Elephant Mine, USA, where
324 schneiderhöhnite coexists with löllingite, arsenopyrite and arsenolite (Smith and Fritzsich 2000).

325 The Szklary pegmatite has numerous droplet inclusions of native As and Sb, stibarsen and
326 paradocrasite, As_2O_3 and Sb_2O_3 oxides, stibiocolumbite and stibiotantalite as Sb^{3+} -(Nb,Ta)
327 oxides, abundant substitution of As^{3+} and Sb^{3+} for Si^{4+} in dumortierite-group minerals (Pieczka
328 2010; Pieczka et al. 2011, 2013), and the presence of schafarzikite, lepageite and other
329 unrecognized arsenite-antimonites. Furthermore, the presence of $\text{As}^{5+} \pm \text{Sb}^{5+}$ in (As,Sb)-bearing
330 pyrochlores and apatites, chernovite-(Y) and arsenogorceixite, is unique. Moreover, the absence
331 of sulfides and arsenides, and the presence of exceptionally rare baryte only in the arsenite-
332 antimonite assemblage, are other important characteristics of the pegmatite.

333 The unique minerals of the Szklary pegmatite allow evaluation of the redox conditions of
334 crystallization using Eh–pH diagrams for such redox-sensitive elements as As, Sb and Fe,

335 approximated to room temperature and $P = 10^5$ Pa (Takeno 2005). Superimposing these diagrams
 336 (Fig. 6) indicates that crystallization of As^{3+} and Sb^{3+} phases containing both Fe^{2+} and Fe^{3+} (as
 337 well as Mn^{2+}) occur at alkaline conditions ($\text{pH} \approx 9\text{--}11$) at relatively low reduction potential ($\text{Eh} \approx$
 338 -0.7 to -0.3 V). This range of pH conditions corresponds to spring waters discharged from rocks
 339 undergoing active serpentinization, which typically have pH values even above 10 (McCollom
 340 and Seewald 2013). Above $\text{Eh} > -0.4$ to -0.3 V, the HAsO_4^{2-} species exists and arsenates should
 341 already crystallize in this pH range; at $\text{pH} < 8$, the $\text{FeOH}^+/\text{Fe}_2\text{O}_3$ and $\text{HAsO}_2/\text{HAsO}_4^{2-}$ equilibria
 342 superimpose, and thus FeOH^+ can only exist along with HAsO_2 with no ferric iron and arsenate
 343 species, or the species should occur together at slightly higher Eh. None of the latter situations
 344 corresponds to the assemblage recorded at Szklary, where tiny crystals of hematite are rarely
 345 associated with lepageite and the unrecognized arsenite-antimonite species as minute inclusions
 346 in (Mn,Be,Na,Cs)-bearing cordierite. The arsenite-antimonite assemblage also cannot crystallize
 347 at $\text{pH} > 11$, because magnetite should crystallize at these conditions (Fig. 6), and it is not
 348 observed at Szklary.

349 The conditions characterized above correspond to As and Sb transported in the alkaline fluids
 350 as H_2AsO_3^- and HSbO_2 species and explain the initial formation of native As and Sb and their
 351 melts at the contacts with a more acidic felsic pegmatite-forming melt via the following redox
 352 reactions:



355 The change in pH caused by the alkaline fluids in the contact zone gave rise to successive
 356 crystallization of arsenite-antimonite phases, and finally to the appearance of As^{5+} - and Sb^{5+} -
 357 bearing species at increasing Eh, observed in the pegmatite only as products of the final
 358 crystallization: AsO_4 -bearing apatite-group minerals, arsenogorceixite, chernovite-(Y), (As,Sb)-

359 bearing pyrochlores, and coexisting baryte as a product of trace precipitation of BaSO₄ from
360 oxidizing fluids carrying accessory sulfate anion. According to this scenario, arsenite-antimonite
361 minerals can occur in granitic pegmatites only as accessory minerals, and this is what is observed.

362

363

Acknowledgements

364 We thank Anthony R. Kampf and an anonymous reviewer for valuable comments on this
365 manuscript. The studies were supported by the National Science Centre (Poland) grant
366 2015/17/B/ST10/03231 to AP and a Discovery Grant to FCH from the Natural Sciences and
367 Engineering Research Council and a Grant from the Canada Foundation for Innovation to FCH.

368

369

References

370 Cassedanne, J.P. (1986) The Urucum pegmatite, Minas Gerais, Brazil. *Mineralogical Record*, 17,
371 307–314.

372 Černý, P., and Ercit, T.S. (2005) The classification of granitic pegmatites revisited. *The Canadian*
373 *Mineralogist*, 43, 2005–2026.

374 Černý, P., Chapman, R., Ferreira, K., and Smeds, S.A. (2004) Geochemistry of oxide minerals of
375 Nb, Ta, Sn, and Sb in the Varuträsk granitic pegmatite, Sweden: The case of an “anomalous”
376 columbite-tantalite trend. *American Mineralogist*, 89, 505–518.

377 Coda, A., Dal Negro, A., Sabelli, C., and Tazzoli, V. (1977) The crystal structure of
378 stenhuggarite. *Acta Crystallographica*, B33, 1807–1811.

379 Cooper, M.A., and Hawthorne, F.C. (1996) The crystal structure of ludlockite, PbFe³⁺₄As³⁺₁₀O₂₂,
380 the mineral with pentameric arsenite groups and orange hair. *The Canadian Mineralogist*, 34,
381 79–89.

382 Cooper, M.A., and Hawthorne, F.C. (2016) Refinement of the crystal structure of
383 schneiderhöhnite. *The Canadian Mineralogist*, 54, 707–713.

384 Deschamps, F., Godard, M., Guillot, S., and Hattori, K. (2013) Geochemistry of subduction zone
385 serpentinites: A review. *Lithos*, 178, 96–127.

386 Gagné, O.C., and Hawthorne, F.C. (2015) Comprehensive derivation of bond-valence parameters
387 for ion pairs involving oxygen. *Acta Crystallographica*, B71, 562–578.

388 Gagné, O. C., and Hawthorne, F.C. (2018) Bond-length distributions for ions bonded to oxygen:
389 Metalloids and post-transition metals. *Acta Crystallographica*, B74, 63-78.

390 Gaines, R.V., Skinner, H.C., Foord, E.E., Mason, B., and Rosenzweig, A. (1997) *Dana's New*
391 *Mineralogy*, 8th ed., John Wiley & Sons, Inc.

392 Larsen, A.O. (2013) Contributions to the mineralogy of the syenite pegmatites in the Larvik
393 Plutonic Complex. *Norsk Bergverksmuseet Skrift*, 50, 101–109.

394 Le Page, Y. (1987) Computer derivation of the symmetry elements implied in a structure
395 description. *Journal of Applied Crystallography*, 20, 264–269.

396 Le Page, Y. (1988) MISSYM 1.1 – a flexible new release. *Journal of Applied Crystallography*,
397 21, 983–984.

398 Majerowicz, A., and Pin, C. (1986) Preliminary trace element evidence for an oceanic depleted
399 mantle origin of the Ślęza ophiolitic complex SW Poland. *Mineralogia Polonica*, 17, 12–22.

400 Mandarino, J.A. (1979) The Gladstone-Dale relationship. Part III. Some general applications. *The*
401 *Canadian Mineralogist*, 17, 71–76.

402 Mandarino, J.A. (1981) The Gladstone-Dale relationship. Part IV. The compatibility concept and
403 its application. *The Canadian Mineralogist*, 19, 441–450.

404 McCollom, T.M., and Seewald, J.S. (2013) Serpentinites, hydrogen, and life. *Elements*, 9, 129–
405 134.

406 Oliver, G.J.H., Corfu, F., and Krogh, T.E. (1993) U–Pb ages from SW Poland: evidence for a
407 Caledonian suture zone between Baltica and Gondwana. *Journal of Geological Society*,
408 London, 150, 355–369.

409 Pieczka, A. (2000) A rare mineral-bearing pegmatite from the Szklary serpentinite massif, the
410 Fore-Sudetic Block, SW Poland. *Geologia Sudetica*, 33, 23–31.

411 Pieczka, A. (2010) Primary Nb-Ta minerals in the Szklary pegmatite, Poland: New insights into
412 controls of crystal chemistry and crystallization sequences. *American Mineralogist*, 95, 1478–
413 1492.

414 Pieczka, A., Grew, E.S., Groat, L.A., and Evans, R.J. (2011) Holtite and dumortierite from the
415 Szklary pegmatite, Lower Silesia, Poland. *Mineralogical Magazine*, 75, 303–315.

416 Pieczka, A., Evans, R.J., Grew, E.S., Groat, L.A., Ma, C., and Rossman, G.R. (2013) The
417 dumortierite supergroup. II. Three new minerals from the Szklary pegmatite, SW Poland:
418 Nioboholtite, $(\text{Nb}_{0.6}\square_{0.4})\text{Al}_6\text{BSi}_3\text{O}_{18}$, titanoholtite, $(\text{Ti}_{0.75}\square_{0.25})\text{Al}_6\text{BSi}_3\text{O}_{18}$, and szklaryite,
419 $\square\text{Al}_6\text{BAS}^{3+}_3\text{O}_{15}$. *Mineralogical Magazine*, 77, 2841–2856.

420 Pieczka, A., Szuszkiewicz, A., Szełęg, E., Janeczek, J., and Nejbert, K. (2015) Granitic
421 pegmatites of the Polish part of the Sudetes (NE Bohemian massif, SW Poland). *Fieldtrip*
422 *Guidebook of the 7th International Symposium on Granitic Pegmatites*, Książ, Poland, June
423 17-19, 2015, C 73–103.

424 Pieczka, A., Biagioni, C., Gołębiowska, B., Jeleń, P., Pasero, M., and Sitarz, M. (2018)
425 Parafiniukite, $\text{Ca}_2\text{Mn}_3(\text{PO}_4)_3\text{Cl}$, a new member of the apatite supergroup from the Szklary
426 pegmatite, Lower Silesia, Poland: Description and crystal structure. *Minerals*, 9, 485.

427 Pouchou, I. L., and Pichoir, F. (1985) “PAP” (phi-rho-z) procedure for improved quantitative
428 microanalysis. In I.T. Armstrong, Ed., *Microbeam Analysis*, pp. 104–106, San Francisco
429 Press, San Francisco.

- 430 Sandström, F. (2008) Varuträskpegmatiten. *Litofilen*, 25(2), 17–46 (in Swedish).
- 431 Sandström, F., and Lahti, S.I. (2009) Viitaniemipegmatiten i Eräjärvi, Orivesi, Finland. *Litofilen*,
- 432 26(1), 11–38.
- 433 Smith, A.E., and Fritsch, E. (2000) South Dakota. *Rock & Minerals*, 75(3), 156–169.
- 434 Strunz, H., and Nickel, E.H. (2001) *Strunz Mineralogical Tables*, 9th Edition. Schweizerbart'sche
- 435 Verlagsbuchhandlung, Stuttgart.
- 436 Szuszkiewicz, A., Pieczka, A., Gołębiowska, B., Dumańska-Słowik, M., Marszałek, M., and
- 437 Szełęg, E. (2018): Chemical composition of Mn- and Cl-rich apatites from the Szklary
- 438 pegmatite, Central Sudetes, SW Poland: Taxonomic and genetic implications. *Minerals*, 8,
- 439 350.
- 440 Takeno, N. (2005): *Atlas of Eh-pH diagrams. Intercomparison of thermodynamic databases.*
- 441 Geological Survey of Japan Open File Report No.419. National Institute of Advanced
- 442 Industrial Science and Technology; Research Center for Deep Geological Environments.
- 443 Timmermann, H., Parrish, R.R., Noble, S.R., and Kryza, R. (2000) New U–Pb monazite and
- 444 zircon data from the Sudetes Mountains in SW Poland: evidence for a single-cycle Variscan
- 445 orogeny. *Journal of the Geological Society, London*, 157, 265–268.
- 446 Turniak, K., Pieczka, A., Kennedy, A.K., Szełęg, E., Ilnicki, S., Nejbart, K., and Szuszkiewicz,
- 447 A. (2015) Crystallisation age of the Julianna pegmatite system (Góry Sowie Block, NE
- 448 margin of the Bohemian massif): evidence from U-Th-Pb SHRIMP monazite and CHIME
- 449 uraninite studies. *Book of Abstracts of the 7th International Symposium on Granitic*
- 450 *Pegmatites*, Książ, Poland, 111–112.
- 451 Van Breemen, O., Bowes, D.R., Aftalion, M., and Żelaźniewicz, A. (1988) Devonian
- 452 tectonothermal activity in the Sowie Góry gneissic block, Sudetes, southwestern Poland:

453 evidence from Rb-Sr and U-Pb isotopic studies. *Journal of Polish Geological Society*, 58, 3–
454 10.

455 Voloshin, A.V., Pakhomovsky, Ya.A. and Bakhchisaraitsev, A.Yu. (1989) On karibibite and
456 schneiderhohnite from pegmatites of Eastern Kazakhstan. *Novye Dannye o Mineralakh*,
457 Moscow, Nauka, 36, 129–135 (in Russian).

458 **Figure captions:**

459 **Figure 1.** Characteristic appearance of lepageite in the Szklary pegmatite: (a) inclusion of the
460 holotype crystal (before extraction) in (Mn,Be,Na,Cs)-bearing cordierite; (b) other representative
461 inclusions of lepageite in cordierite; (c) holotype lepageite. Abbreviations: Crd – cordierite, Hrm
462 – harmotome, Qz – quartz.

463

464 **Figure 2.** The $[\text{Sb}_4\text{As}_4\text{O}_{19}]$ cluster in the crystal structure of lepageite.

465

466 **Figure 3.** Components of the structure of lepageite: (a) the cluster of Mn^{2+}O_7 groups (blue
467 polyhedra) and Mn^{2+}O_8 groups (lilac polyhedra); (b) the trimer of Fe^{2+}O_6 octahedra (yellow
468 polyhedra).

469

470 **Figure 4.** Components of the structure of lepageite: (a) the extended linkage of Fe^{2+}O_6 octahedra.

471 Legend as in Fig. 2.

472

473 **Figure 5.** The crystal structure of lepageite; legend as in Fig. 2 plus green circles: Sb^{3+} ; red
474 circles: As^{3+} .

475

476 **Figure 6.** Crystallization conditions for arsenite-antimonite minerals in the Szklary pegmatite
477 shown in the Eh–pH diagrams of Takeno (2005). The Eh–pH relations for Fe are marked in
478 black, for As in orange, and for Sb in green. Manganese is omitted because it occurs as Mn^{2+} at
479 pH < 10.5 and Eh < 0.2 V.

480
481

Table 1. Minerals of the Szklary pegmatite containing As and Sb.

Mineral	Formula
Metalloids	
Arsenic	As
Antimony	Sb
Stibarsen	AsSb
Paradocrasite	Sb ₃ As
Oxides and hydroxides	
Arsenolite / claudetite	As ₂ O ₃
Senarmontite	Sb ₂ O ₃
Stibiocolumbite	SbNbO ₄
Stibiotantalite	SbTaO ₄
Oxy-stibiomicrolite	(Sb ³⁺ ,Ca) ₂ Ta ₂ O ₆ O
Calciobetafite (Sb-bearing)	(Ca,Sb ³⁺ ,□) ₂ (Ti,Sb ⁵⁺ ,Nb) ₂ (O,OH,□)
a U-Mn-As-Sb-Ta-Ti oxide	[(Mn,Fe) _{<3} U _{>1}] _{Σ4} (As ₂ Sb ₂) _{Σ4} [(Ta,Nb) _{>2} Ti _{<2}] _{Σ4} O ₂₀
Arsenites and antimonites	
Schafarzikite	FeSb ₂ O ₄
Lepageite	Mn ²⁺ ₃ (Fe ³⁺ ₇ Fe ²⁺ ₄)O ₃ [Sb ³⁺ ₅ As ³⁺ ₈ O ₃₄]
Phosphates and arsenates	
Fluorapatite (Mn,As-bearing)	(Ca,Mn) ₅ [(P,As)O ₄] ₃
Pieczkaite (As-bearing)	Mn ₅ [(P,As)O ₄] ₃
Chernovite-(Y)	YAsO ₄
Arsenogorceixite	BaAl ₃ (AsO ₄)(AsO ₃ OH)(OH) ₆
Silicates	
Dumortierite (As,Sb-bearing)	Al _{7-(5x+4w+y)/3} (Ta,Nb) _x Ti _w □ _{(2x+w+y)/3} BSi _(3-y) (Sb,As) _y O _{18-y} y ≤ 1.5 and 1-(5x+4w+y)/3 > x and > y
Holtite (As,Sb-bearing)	Al _{7-(5x+4w+y)/3} (Ta,Nb) _x Ti _w □ _{(2x+w+y)/3} BSi _(3-y) (Sb,As) _y O _{18-y} y ≤ 1.5 and x > 1-(5x+4w+y)/3 and > w and Ta > Nb
Nioboholtite (As,Sb-bearing)	Al _{7-(5x+4w+y)/3} (Ta,Nb) _x Ti _w □ _{(2x+w+y)/3} BSi _(3-y) (Sb,As) _y O _{18-y} y ≤ 1.5 and x > 1-(5x+4w+y)/3 and > w and Ta < Nb
Titanoholtite (As,Sb-bearing)	Al _{7-(5x+4w+y)/3} (Ta,Nb) _x Ti _w □ _{(2x+w+y)/3} BSi _(3-y) (Sb,As) _y O _{18-y} y ≤ 1.5 and w > 1-(5x+4w+y)/3 and > x
Szklaryite*	Al _{7-(5x+4w+y)/3} (Ta,Nb) _x Ti _w □ _{(2x+w+y)/3} BSi _(3-y) (Sb,As) _y O _{18-y} y > 1.5

482 * classified within the dumortierite supergroup. Because the formulas of dumortierite-supergroup
483 end-members do not reflect common presence of Sb + As in compositions of the supergroup
484 minerals, the formulas of the minerals are presented in the form of the general supergroup
485 formula (Pieczka et al. 2013) and additional relationships among the contents of Al, Nb+Ta and
486 Ti at the Al1 site and Sb+As at the Sb(As) site of the dumortierite structure, which must be
487 fulfilled for each of the minerals.
488

489 Table 2. Chemical composition of lepageite.

490

constituent	Mean (wt%)	Range (wt%)	sd (wt%)	cation	<i>apfu</i>	sd (apfu)
As ₂ O ₃	31.62	30.83 – 32.44	0.66	As ³⁺	8.32	0.17
Sb ₂ O ₃	26.23	25.05 – 27.35	0.94	Sb ³⁺	4.68	0.17
Fe ₂ O ₃	21.17	20.64 – 21.58	0.41	Fe ³⁺	6.90	0.13
FeO*	10.74	9.45 – 11.75	1.07	Fe ²⁺	3.89	0.39
MnO	8.44	7.88 – 9.27	0.59	Mn ²⁺	3.10	0.22
MgO	0.26	0.18 – 0.33	0.06	Mg ²⁺	0.16	0.04
Total	98.46					

491 Notes: *total Fe as FeO (mean 29.79% FeO); sd – standard deviation.

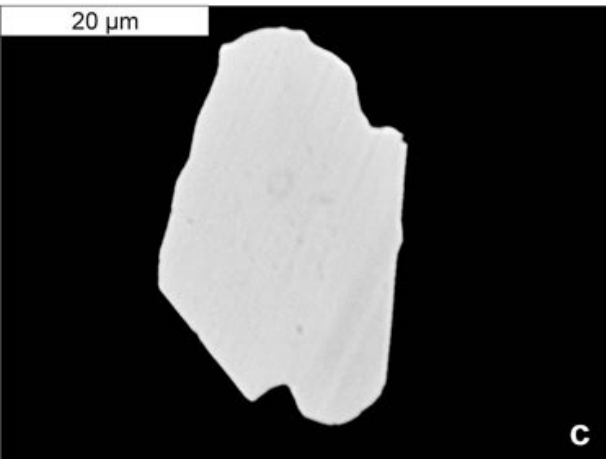
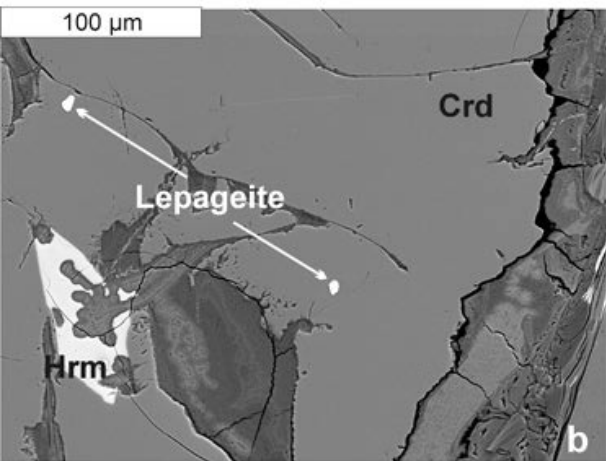
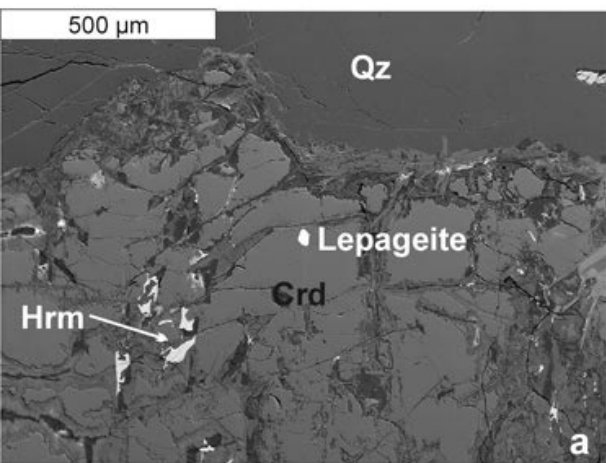
Table 3. Generated powder diffraction pattern for lepageite
(the strongest reflection are marked in bold)

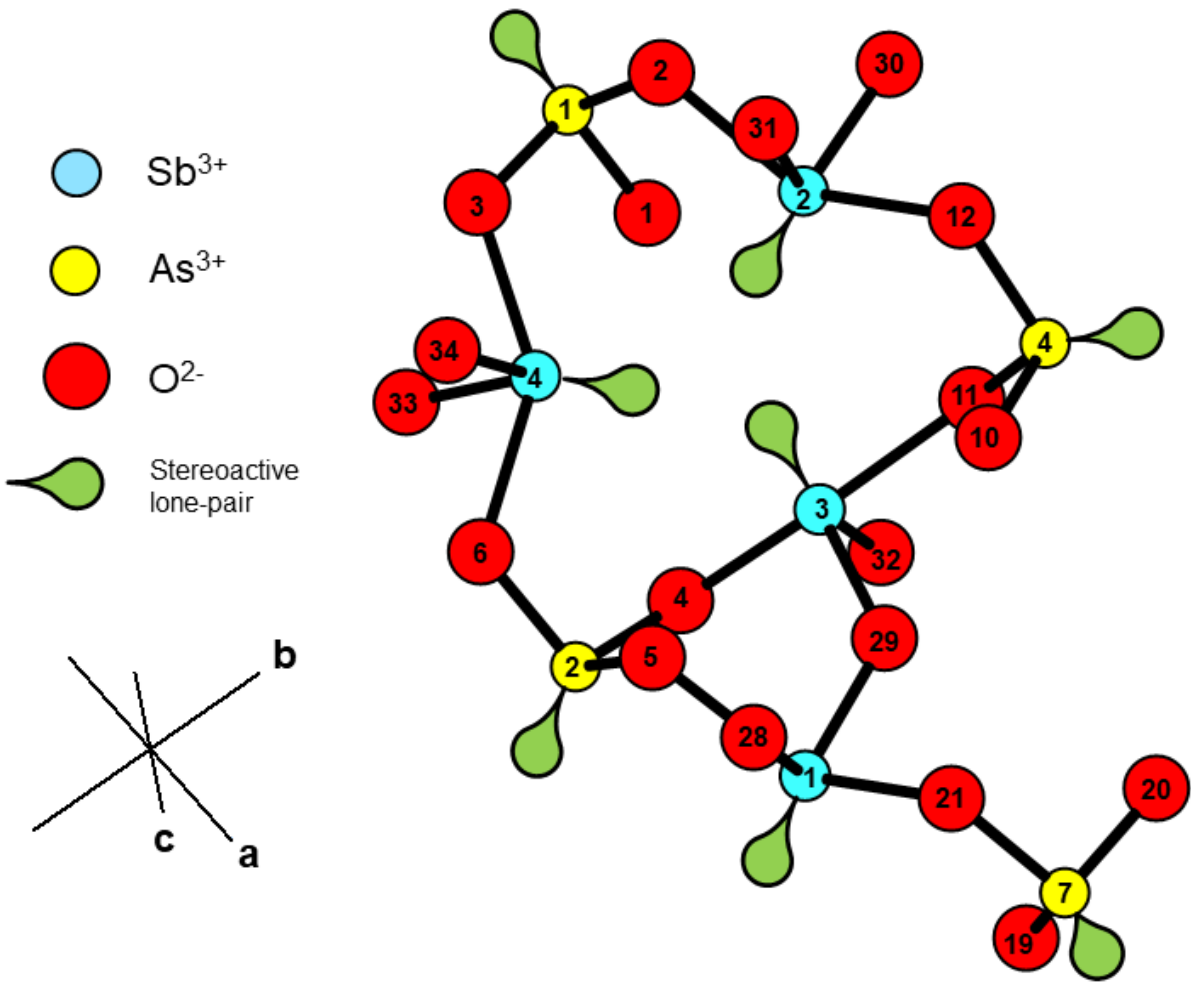
<i>I</i> (%)	<i>d</i> (Å)	<i>h k l</i>	<i>I</i> (%)	<i>d</i> (Å)	<i>h k l</i>
2	8.563	0 1 1	100	2.831	0 -3 3
2	7.348	1 1 0	2	2.785	-2 -1 5
3	6.866	-1 0 2	2	2.735	-3 2 3
2	5.746	-1 1 2	2	2.703	2 -2 3
3	5.221	0 2 0	2	2.638	-4 0 2
2	4.811	1 1 2	3	2.617	2 1 4
2	4.595	-2 1 0	2	2.610	0 4 0
2	4.463	-1 -1 3	2	2.568	4 0 0
3	4.321	1 2 1	2	2.553	-4 0 3
6	4.104	-2 0 3	34	2.487	-3 -3 1
10	3.791	-1 0 4	34	2.474	-3 3 1
4	3.770	1 2 2	34	2.463	0 0 6
6	3.732	1 -2 2	2	2.246	3 0 4
3	3.543	-2 -2 2	3	2.234	-4 0 5
11	3.539	-2 2 2	3	2.226	-3 -3 4
11	3.535	-3 0 1	2	2.206	1 4 3
2	3.423	3 0 0	3	2.141	0 4 4
2	3.354	-3 -1 1	2	2.123	0 -4 4
2	3.275	-3 1 2	2	2.108	-5 0 1
2	3.273	-1 3 1	2	2.091	-5 0 3
2	3.260	3 1 0	3	2.074	4 0 3
3	3.228	1 0 4	2	2.023	-5 0 4
4	3.224	-2 -2 3	2	1.889	2 -5 1
5	3.179	2 0 3	2	1.853	-1 3 7
2	3.176	1 3 1	17	1.768	-4 2 7 / -6 0 2
5	3.050	2 1 3 / -1 0 5	2	1.766	-4 -3 6
2	3.028	0 2 4	18	1.763	-3 3 7
2	2.955	0 0 5	19	1.756	-3 -3 7
2	2.933	-1 1 5	21	1.744	3 3 5
85	2.898	-3 0 4	23	1.740	0 6 0
2	2.893	-2 0 5	24	1.728	3 -3 5
3	2.891	2 3 0	2	1.697	-2 5 5
4	2.872	3 2 0 / -2 3 0	2	1.674	-6 0 5
92	2.854	0 3 3	2	1.654	6 0 1
88	2.846	3 0 2	2	1.648	5 3 2

Table 4. Bond-valence table* for lepageite

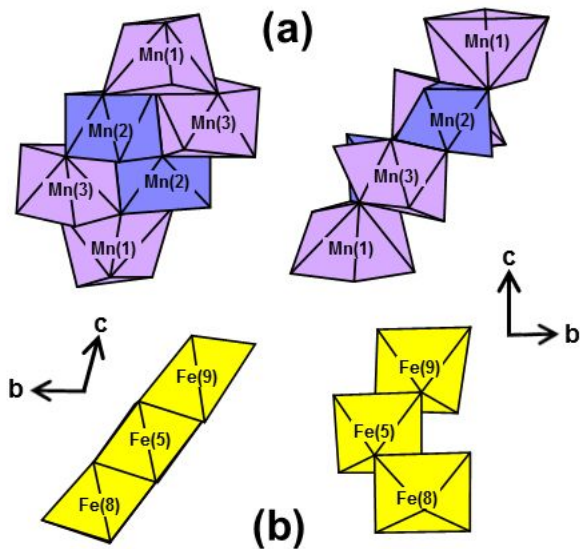
	Sb(1)	Sb(2)	Sb(3)	Sb(4)	As(1)	As(2)	As(3)	As(4)	As(5)	As(6)	As(7)	As(8)**	As(9)	Mn(1)	Mn(2)	Mn(3)	Fe(1)	Fe(2)	Fe(3)	Fe(4)	Fe(5)	Fe(6)	Fe(7)	Fe(8)	Fe(9)	Fe(10)	Fe(11)	Σ	
O(1)		0.07		0.09	1.17	0.03	0.03	0.03																0.56				1.99	
O(2)		0.47			0.89																	0.38					0.23	1.97	
O(3)				0.55	0.87																					0.22		2.05	
O(4)			0.49	0.05		1.02				0.03																0.36		1.95	
O(5)	0.41		0.08			0.98											0.56											2.03	
O(6)				0.38		0.92														0.39					0.23			1.92	
O(7)							0.99									0.11			0.39									1.85	
O(8)							0.92										0.46							0.18				1.89	
O(9)							0.88													0.39						0.27		1.94	
O(10)			0.07				0.03	1.06							0.25				0.54									1.95	
O(11)		0.05	0.45					1.06	0.03																		0.37	1.96	
O(12)		0.43						0.84																				1.89	
O(13)									1.00					0.36	0.28	0.27									0.26			1.91	
O(14)									1.00																			2.00	
O(15)									0.99			0.04		0.11									0.56			0.26		2.06	
O(16)	0.07									1.04				0.41									0.54		0.46		0.38	1.91	
O(17)										1.01		0.05		0.05							0.54						0.37	2.02	
O(18)										0.99		0.05									0.54					0.38		1.96	
O(19)	0.12										1.10					0.04									0.68			1.88	
O(20)							0.06				1.09			0.40	0.33													2.02	
O(21)	0.64										0.93															0.29		2.02	
O(22)												0.93										0.44					0.30	1.88	
O(23)												0.91									0.24		0.36					1.85	
O(24)												0.89											0.42				0.31	1.86	
O(25)													1.02	0.16		0.42								0.43					
O(26)			0.05										0.90				0.57	0.50											
O(27)													0.87			0.12		0.45				0.56							
O(28)	0.82																0.47							0.29		0.33		1.91	
O(29)	0.81		0.84											0.04	0.35													2.04	
O(30)		0.99																							0.46		0.43	1.94	
O(31)		0.86																				0.60	0.60						
O(32)			0.88											0.32													0.36	0.36	1.92
O(33)				0.97																					0.48		0.43		1.93
O(34)				0.88																	0.63	0.61							2.11
O(35)													0.10				0.60			0.71				0.49				1.90	
O(36)															0.28	0.43		0.74								0.51		1.96	
O(37)													0.03	0.42								0.76		0.69				1.90	
Σ	2.87	2.93	2.86	2.97	2.93	2.95	2.91	2.99	3.02	3.07	3.12	2.87	3.00	1.87	1.92	1.90	2.99	2.98	2.90	2.94	2.84	2.87	2.53	2.33	2.04	2.04	2.08		

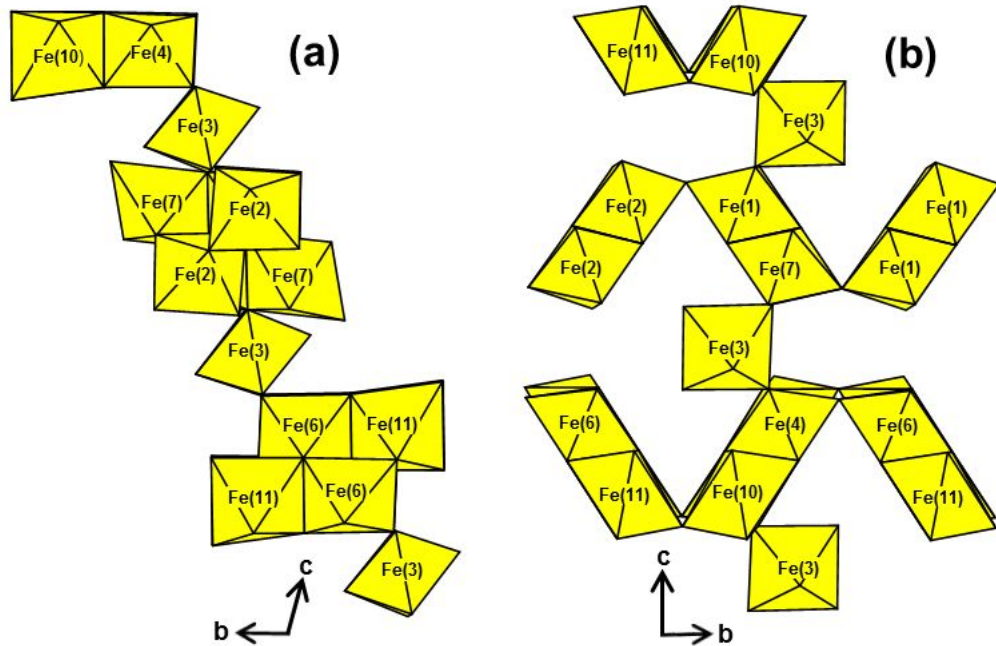
*Bond valences in *vu* (valence units), bond-valence parameters from Gagné and Hawthorne (2015).
**As(8) site-occupancy (As_{0.637}Sb_{0.363}).





6903_Pieczka et al._Lepageite_Fig3_R1





6903_Pieczka et al._Lepageite_Fig5_R1

